Journal of Inflammation Research

Dovepress
Taylor & Francis Group

Open Access Full Text Article

ORIGINAL RESEARCH

Zuo Gui Wan Promotes Remyelination in Multiple Sclerosis by Attenuating MAPK-Mediated Microglial M1 Polarization, an Integrated Network Pharmacology and Experimental Validation Study

Peiyuan Zhao[1–3,*], Yihao Li[1,*], Wenlu Li[1], Xu Han[1], Wen Cheng[1], Mengyang Fan[1], Liuqing Xu[1], Jingxian Han[4], Xihong Liu[1]

[1]Henan University of Chinese Medicine, Zhengzhou, Henan, People's Republic of China; [2]Collaborative Innovation Center for Prevention and Treatment of Major Diseases by Chinese and Western Medicine, Zhengzhou, Henan, People's Republic of China; [3]Collaborative Innovation Center of Research and Development on the Whole Industry Chain of Yu-Yao, Zhengzhou, Henan, People's Republic of China; [4]The 7th People's Hospital of Zhengzhou, Zhengzhou, Henan, People's Republic of China

*These authors contributed equally to this work

Correspondence: Xihong Liu, Traditional Chinese Medicine (Zhong Jing) School, Henan University of Chinese Medicine, No. 156, Jinshui East Road, Zhengdong New District, Zhengzhou, Henan, 450046, People's Republic of China, Tel +86 15810191601, Email lxhong423@hactcm.edu.cn

Purpose: Zuo Gui Wan (ZGW) shows clinical potential in treating multiple sclerosis (MS), but its underlying mechanism of action remains elusive. This study aims to elucidate the efficacy and molecular mechanisms of ZGW in a cuprizone (CPZ)-induced demyelination mouse model.

Methods: Adult male C57BL/6J mice were randomized into four groups (n = 12 each), normal control (NC), CPZ model, CPZ + 2.8 g/kg/d ZGW (ZGW-L), and CPZ + 5.6 g/kg/d ZGW (ZGW-H). Demyelination was induced by a 0.2% CPZ diet for 9 weeks. ZGW or saline was administered intragastrically from weeks 6 to 9. Behavioral performance was assessed using the rotarod, elevated plus-maze, and tail suspension tests. Remyelination was evaluated via LFB staining, TEM, and the expression of oligodendrocyte markers (Olig2, CNPase, MOG). Microglial activation/polarization (Iba-1, iNOS, CD86, Arg-1, CD206) and MAPK pathway proteins (p-ERK1/2, p-p38, and p-JNK) were quantified by Western blot or immunofluorescence. The phytochemical profile of ZGW were analyzed using LC-MS, and target prediction was performed using TCMSP, BATMAN-TCM, and SwissTarget Prediction. Network pharmacology, protein-protein interaction (PPI) analysis, and molecular docking were employed to identify core pathways and targets.

Results: ZGW treatment exhibited a dose-dependent improvement in motor coordination and alleviated anxiety- and depression-like behaviors in CPZ mice. Histological and ultrastructural analyses demonstrated significantly enhanced remyelination and increased expression of Olig2, CNPase, and MOG. Network pharmacology and molecular docking analyses identified the MAPK signaling cascade as the principal therapeutic axis, with key ZGW compounds showing high affinity for MAPK3 and TNF-α. In vivo, ZGW suppressed CPZ-induced phosphorylation of ERK1/2, p38, and JNK, reduced Iba-1 expression and M1 markers (iNOS and CD86), but did not significantly alter Arg-1 or CD206.

Conclusion: ZGW promotes remyelination in CPZ-induced demyelination by inhibiting MAPK pathway overactivation and attenuating microglial M1 polarization, thereby modulating the neuroinflammatory milieu.

Keywords: remyelination, microglial polarization, MAPK signaling pathway, traditional Chinese medicine formula

Introduction

Multiple sclerosis (MS) is an immune-mediated inflammatory demyelinating disorder of the central nervous system (CNS), characterized by focal demyelination in both white and gray matter, axonal loss, and perivascular inflammation.[1,2] It is estimated that over 2.2 million people worldwide are affected by MS, making it a major cause of neurological

https://doi.org/10.2147/JIR.S572873
Received: 10 October 2025
Accepted: 13 January 2026
Published: 5 February 2026

Graphical Abstract

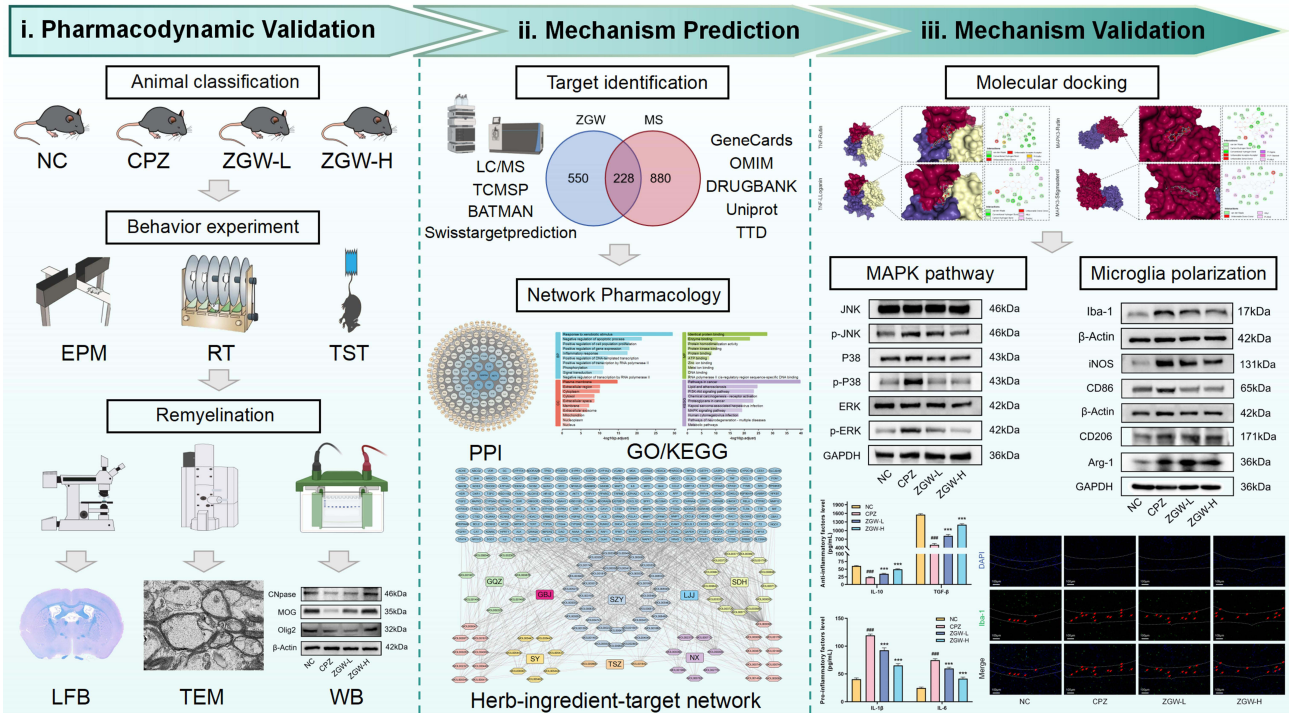

dysfunction in young adults.[3] The predominant disease type is relapsing-remitting MS, which follows a course of acute exacerbations followed by recovery phases.[4] Acute relapses are typically treated with high-dose methylprednisolone or prednisone acetate, whereas long-term disease management relies on disease-modifying therapies (DMT), including teriflunomide, fingolimod hydrochloride, siponimod, and dimethyl fumarate.[5,6] Although DMTs are effective in reducing relapse rates and delaying disability progression, their long-term use is often limited by adverse effects such as gastrointestinal disturbances and hepatotoxicity.[7] Consequently, there is growing interest in exploring traditional medicine-based interventions, including Traditional Chinese Medicine (TCM), as alternative or complementary therapies, offering potentially safer options for a broader spectrum of MS patients.

Zuo Gui Wan (ZGW) is a classical TCM formula first documented in *Jingyue Quanshu* by Zhang Jingyue during the Ming Dynasty. It comprises eight components, *Dioscoreae Rhizoma* (Shan Yao, SY), *Rehmanniae Radix Preparata* (Shu Di Huang, SDH), *Achyranthes Bidentatae Radix* (Niu Xi, NX), *Corni Fructus* (Shan Zhu Yu, SZY), *Lycii Fructus* (Gou Qi Zi, GQZ), *Cuscutae Semen* (Tu Si Zi, TSZ), *Testudinis Carapax et Plastrum* (Gui Ban Jiao, GBJ), and *Cervi Cornus Colla* (Lu Jiao Jiao, LJJ). According to TCM theory, ZGW is renowned for its yin-tonifying and kidney-nourishing actions. It is traditionally prescribed to alleviate Kidney deficiency, such as physical weakness, fatigue, and visual disturbances, which parallel certain manifestations of MS. The canonical TCM text *Lingshu·Hailun* states that "the Kidneys govern the bones and generate the marrow". Furthermore, TCM theory posits that "the brain is the sea of marrow". This conceptual framework suggests that reinforcing the Kidney can promote marrow regeneration and nourish the brain, thereby positioning ZGW as a promising candidate for MS treatment.[8]

Remyelination is essential for restoring neurological function in MS. However, the clinical translation of remyelination therapies remains a significant challenge. A primary reason for the failure of previous candidates is that they often target oligodendrocyte precursor cells (OPCs) directly without addressing the hostile inflammatory microenvironment that arrests their maturation. Specifically, an imbalance in microglial polarization represents a major obstacle to effective myelin repair.[9] While microglia can adopt a pro-reparative M2 phenotype, in chronic MS, they often become locked in a

persistent pro-inflammatory M1 state - a pathological condition frequently described as "chronic activation" or "microglial aging". This sustained M1 polarization creates a hostile niche that not only impedes OPC differentiation but also impairs the clearance of inhibitory myelin debris, rendering pure OPC-targeting therapies ineffective.[9,10] Therefore, therapeutic strategies capable of simultaneously modulating the immune microenvironment and fostering repair are urgently needed. Existing experimental evidence demonstrates that ZGW significantly increases myelin basic protein (MBP) expression in an experimental autoimmune encephalomyelitis (EAE) model, indicating its potential to promote remyelination.[8] In addition, ZGW has been shown to exert neuro-immune modulatory effects.[11] Given this dual potential to modulate inflammation and promote repair, we hypothesized that ZGW ameliorates MS pathology by enhancing remyelination through the regulation of microglial polarization states.

In this study, we utilized a cuprizone (CPZ)-induced demyelination model, which is characterized by corpus callosum demyelination and microglial activation, to evaluate the therapeutic efficacy of ZGW.[12] Furthermore, we employed an integrative research approach combining Liquid Chromatography-Mass Spectrometry (LC-MS), network pharmacology, molecular docking and experimental validation to elucidate the underlying mechanisms of ZGW. This study aims to provide a comprehensive theoretical foundation for the clinical application of ZGW in MS and contribute to the development of novel remyelination therapies.

Materials and Methods

Chemicals and Reagents

ZGW (Product No., Z41020696; Batch No., 20035036) was supplied by Zhongjing Wanxi Pharmaceutical Co., Ltd. (Henan, China). The ZGW pills were ground into a fine powder and suspended in physiological saline. CPZ (purity ≥95%) was sourced from Sigma-Aldrich Co. (St. Louis, MO, USA; Cat#C9012). CPZ was incorporated into standard rodent chow at a concentration of 0.2% by SBF Biotechnology Co., Ltd. (Beijing, China) and sterilized by cobalt-60 γ-irradiation. Mouse ELISA kits for TNF-α (YJ002095), IL-1β (YJ301814), IL-6 (YJ098430), PGE2 (YJ037542), TGF-β (YJ057830), and IL-10 (YJ037873) were procured from Shanghai Enzyme Linked Biotechnology Co., Ltd. (Shanghai, China). Primary antibodies were as follows, MOG (Abcam, AB242374), CNPase (Santa Cruz, sc-166558), Olig2 (Merck, AB9610), Iba-1 (Hunan Aifang, AFW12391), β-actin (Proteintech, 66009-1-Ig), iNOS (Proteintech, 22226-1-AP), CD86 (Proteintech, 26903-1-AP), Arg-1 (Proteintech, 16001-1-AP), CD206 (Proteintech, 18704-1-AP), ERK1/2 (Proteintech, 16443-1-AP), p-ERK1/2 (Proteintech, 28733-1-AP), GAPDH (Servicebio, GB11002-100), p38 (CST, 9212S), p-p38 (CST, 4511S), JNK (CST, 9252S), and p-JNK (CST, 4668S). The Luxol Fast Blue (LFB) Staining Kit (S0192) was obtained from Beijing Biosynthesis Biotechnology Co., Ltd. (Beijing, China). All reagents were stored according to the manufacturer's specifications.

Animal Experimentation

Animal Experimental Design

This study was approved by the Experimental Animal Welfare and Ethics Committee of Henan University of Chinese Medicine (Ethics Approval Code, DWLL202103124). Animal care and experimental procedures were performed in strict accordance with the *Guide for the Care and Use of Laboratory Animals* (8th edition, National Academies Press). We also declare that this study adhered to the ARRIVE guidelines 2.0. Male C57BL/6J mice (8 weeks old, 20 ± 2 g, License, SCXK(Zhe) 2020–0002) were purchased from Vital River Laboratory Animal Technology Co., Ltd. (Zhejiang, China) and housed under standard conditions (22 ± 2°C, 50 ± 10% RH, light-dark cycle for 12 h) with free access to chow and water. After one week of acclimation, 48 mice were randomly divided into four groups (n = 12 per group), normal group (NC), CPZ group (CPZ), low-dose ZGW group (ZGW-L, 2.8 $g \cdot kg^{-1} \cdot d^{-1}$), and high-dose ZGW group (ZGW-H, 5.6 $g \cdot kg^{-1} \cdot d^{-1}$). The CPZ, ZGW-L, and ZGW-H groups were fed a 0.2% CPZ diet for 9 weeks. From week 6 to week 9, ZGW-L and ZGW-H received ZGW intragastrically once daily; NC and CPZ groups received equal volumes of saline. At the experimental endpoint, mice were anesthetized and subjected to one of three terminal procedures, perfusion with 4% paraformaldehyde (PFA) for LFB staining and Immunofluorescence (IF); perfusion with 2.5% glutaraldehyde for

transmission electron microscopy (TEM); or rapid brain dissection for Western Blotting (WB) and Enzyme-linked immunosorbent assay (ELISA) (tissues stored at –80 °C).

Rotarod Test

Motor coordination and endurance were assessed using an accelerating rotarod (4–40 rpm over 300 s). Each mouse underwent three trials; the latency to fall was averaged.

Elevated Plus Maze (EPM)

Anxiety-like behavior was evaluated on a plus-shaped maze with two open and two closed arms. Mice were placed on the central platform facing an open arm and their movement was recorded for 5 min.

Tail Suspension Test (TST)

Depressive-like behavior was assessed by suspending mice by the tail (adhesive tape placed 2 cm from the tip) from a horizontal bar 30 cm above the bench. After a 1 min habituation, the total duration of immobility was recorded over 5 min. If the mouse attempted to escape by climbing its tail, the experiment was invalid.

LFB Staining

Paraffin-embedded brain sections were dewaxed, rehydrated, and incubated in LFB solution at 56°C for 12 h. Sections were differentiated in 0.05% lithium carbonate solution until the background was colorless, followed by counterstained with eosin. Sections were dehydrated, cleared, and mounted. Myelin integrity was quantified as the percentage of LFB-positive area in the corpus callosum using Image Pro-Plus 6.0.

TEM

Corpus callosum tissue blocks (1 mm^3) were fixed in 2.5% glutaraldehyde, post-fixed with 1% osmium tetroxide, dehydrated, and embedded in Spurr's resin. Target areas were located using semi-thin sections, and then ultrathin sections (60–80 nm) were prepared. Following double staining with uranyl acetate and lead citrate, sections were examined using a JEOL JEM-1230 transmission electron microscope. Myelin ultrastructure was quantified using Image Pro-Plus 6.0 software. The G-ratio was calculated as the ratio of the inner axonal diameter to the total outer diameter of the myelinated fiber. A minimum of 90 randomly selected axons were analyzed per experimental group, with at least 3 mice per group.

WB

Corpus callosum tissues were homogenized in ice-cold RIPA buffer supplemented with phosphatase and protease inhibitors. Protein concentration was determined using the bicinchoninic acid (BCA) assay. Equal amounts of protein were separated via sodium dodecyl sulfate-polyacrylamide gel electrophoresis (SDS-PAGE) and transferred onto polyvinylidene fluoride (PVDF) membranes. Membranes were blocked with 5% non-fat milk for 1 h at room temperature to prevent non-specific binding, followed by overnight incubation at 4°C with primary antibodies against Iba-1 (1:2000), iNOS (1:2000), CD86 (1:1000), CD206 (1:1000), Arg-1 (1:5000), CNPase (1:1000), MOG (1 μg/mL), Olig2 (1:2000), ERK1/2 (1:2000), p-ERK1/2 (1:2000), p38 (1:3000), p-p38 (1:3000), JNK (1:2000), p-JNK (1:2000), β-actin (1:5000) and GAPDH (1:5000). The next day, membranes were incubated with horseradish peroxidase (HRP)-conjugated secondary antibodies for 1 h at room temperature. Protein bands were visualized using enhanced chemiluminescence reagent and quantified using Image Pro-Plus 6.0 software. Phosphorylation proteins (p-ERK1/2, p-JNK, and p-p38) were normalized to their total protein levels, while other proteins were normalized to β-actin or GAPDH.

ELISA

Serum samples and corpus callosum homogenates were assayed for TNF-α, IL-1β, IL-6, PGE2, TGF-β, and IL-10 concentrations according to the manufacturer's instructions. Absorbance was measured at 450 nm using a microplate reader.

Immunofluorescence

Paraffin sections were deparaffinized, rehydrated, and antigen-retrieved in sodium citrate buffer (10 mM, pH 6.0) at 95 °C for 15 min. After PBS washes, sections were blocked in 5% BSA/0.3% Triton X-100 for 1 h. Primary antibody

incubation was performed by applying diluted anti-IBA-1 (1:300) at 4°C overnight. Following washes, sections were incubated with Alexa Fluor-conjugated secondary antibodies (1:500) for 1 h at room temperature, counterstained with DAPI (0.5 μg/mL) for 10 min, and mounted with anti-fade mounting medium. All slides were stored protected from light, and images were acquired within 24 h using a fluorescence microscope, positive cells were quantified in five random fields per section.

Statistical Analysis

Statistical analyses were performed in GraphPad Prism 9.0 using one-way ANOVA followed by Tukey's post-hoc test. The normality of data distribution and homogeneity of variances were confirmed before ANOVA. All experimental results are presented as mean ± standard deviation (SD). P-value < 0.05 was considered statistically significant. All data represents at least three independent experiments.

Network Pharmacology Analysis

Liquid Chromatography-Mass Spectrometry (LC-MS) Profiling

ZGW powder was extracted in 10 volumes of methanol, followed by ultrasonication in a water bath for 30 min. The supernatant was filtered through a 0.22 μm membrane. Chromatographic separation was performed on a Thermo Scientific C18 column (2.1 mm internal diameter) with a mobile phase A (0.1% formic acid in water) and B (methanol). The gradient elution program was set as follows, 0–5 min, 98% A; 5–7 min, 98%→90% A; 7–11 min, 90% A; 11–13 min, 90%→70% A; 13–16 min, 70% A; 16–18 min, 70%→50% A; 18–22 min, 50% A; 22–23 min, 50%→20% A; 23–26 min, 20% A; 26–26.1 min, 20%→98% A; 26.1–30 min, 98% A. The flow rate was maintained at 0.2 mL/min with a column temperature of 30°C and an injection volume of 4 μL.

Mass spectrometric analysis was conducted using an Ultimate 3000 UHPLC system coupled to an Orbitrap Exploris™ 240 (Thermo Scientific). Data were acquired in alternating positive/negative modes at spray voltages of +3.5 kV (positive) and −3.0 kV (negative) with sheath gas 25 arb, auxiliary gas 10 arb, sweep gas 1 arb; ion transfer tube and heater at 350 °C. Full MS was run at 60000 resolution covered m/z 100–1400, data-dependent MS^2 at 15,000 resolution with stepped HCD energies of 30, 50, and 70 eV. Raw data were processed in Compound Discoverer™ 3.3 and Xcalibur™ 4.5 SP1 software (Thermo Scientific) for ingredient analysis and quality control.

ZGW Targets Prediction

The targets of identified ZGW ingredients were predicted using Traditional Chinese Medicine Systems Pharmacology Database and Analysis Platform (TCMSP, https://www.tcmsp-e.com/), BATMAN-TCM (http://bionet.ncpsb.org.cn/), and SwissTargetPrediction (http://swisstargetprediction.ch/). Resulting target names were standardized via UniProt database (http://beta.uniprot.org/) to obtain official gene symbols.

Identification of MS-Related Targets

"Multiple sclerosis" was used as a keyword to retrieve disease-associated targets from Genecards (https://www.genecards.org), Drugbank (https://go.drugbank.com), OMIM (http://www.omim.org), TTD (https://db.idrblab.net/ttd), and PharmGKB (https://www.pharmgkb.org) databases. The intersection of ZGW targets and MS-related genes was determined, and a Venn diagram was generated to visualize shared targets.

Protein-Protein Interaction (PPI) Network Construction and Hub Target Screening

Overlapping targets were uploaded to STRING database (https://string-db.org/). A PPI network was built with confidence interactions ≥0.700. The network was imported into Cytoscape 3.10.2, and the CytoHubba plugin was used to calculate degree centrality, betweenness centrality and closeness centrality. The top 20 genes from each metric were intersected to identify the core targets.

Herbs-Ingredients-Targets Network

A tripartite network linking ZGW herbs, their active ingredients, and shared targets was visualized in Cytoscape 3.10.2. Node degree values were computed via CytoHubba, and the top ten ingredients by degree were highlighted as key bioactives.

Gene Ontology (GO) and Kyoto Encyclopedia of Genes and Genomes Enrichment Analysis (KEGG) Enrichment Analysis

GO and KEGG pathway enrichment analyses of the common targets were performed using the David database (https://david.ncifcrf.gov/) with a significance threshold of $P < 0.01$, and the results were visualized using an online platform (http://www.bioinformatics.com.cn).

Molecular Docking

Three-dimensional structures of core target proteins were downloaded from RCSB PDB (https://www.rcsb.org/). Key active ingredients were retrieved from PubChem (https://pubchem.ncbi.nlm.nih.gov/) in SDF format. Protein and ligand files were submitted to CB-Dock2 (https://cadd.labshare.cn/cb-dock2/) for Structure-based Blind Docking analysis, with visualization of the docking results based on AutoDock Vina. Binding poses and interactions were analyzed and visualized using Discovery Studio 2019.

Results

ZGW Improves Behavioral Performance in CPZ-Induced Demyelinated Mice

To evaluate the therapeutic efficacy of ZGW, we established a CPZ-induced demyelinated mouse model (experimental design detailed in Figure 1A). Animals were randomized into four groups, NC, CPZ, ZGW-L and ZGW-H. Except for the NC group, all groups were fed a diet containing 0.2% CPZ for 9 weeks. Starting from week 6, the ZGW-L and ZGW-H groups received daily intragastric administration of ZGW at 2.8 g/kg and 5.6 g/kg, respectively. Body weight monitoring and behavioral tests, including the EPM, rotarod, and TST, were conducted as shown in Figure 1B–G.

Following the intervention period, both ZGW-treated groups exhibited significantly attenuated CPZ-induced weight loss compared to the CPZ model group ($P < 0.05$), with ZGW-H showing a more pronounced improvement. In the EPM test, CPZ mice exhibited fewer open-arm entries and reduced time spent in open arms compared to the NC group ($P < 0.05$), indicative of heightened anxiety-like behavior. Similarly, rotarod performance was impaired, as evidenced by a shorter latency to fall ($P < 0.05$), and TST immobility time was prolonged ($P < 0.01$), reflecting motor coordination deficits and depressive-like behavior, respectively. Treatment with ZGW significantly reversed these behavioral deficits. Both ZGW doses increased the percentage of open-arm entries and duration in the EPM, prolonged rotarod fall latency, and reduced TST immobility ($P < 0.01$), with ZGW-H showing the most pronounced improvements. These data demonstrate that ZGW alleviates CPZ-induced neurobehavioral impairments in a dose-dependent manner.

ZGW Promotes Remyelination in CPZ-Induced Demyelinated Mice

To confirm the remyelination-promoting effects of ZGW, we performed LFB staining, TEM and WB analysis of myelin markers in the corpus callosum. LFB staining revealed a significant reduction in the myelin-positive area in CPZ mice versus NC ($P < 0.001$). Conversely, the ZGW-H group exhibited a significant increase in the myelin-positive area relative to the CPZ group ($P < 0.001$; Figure 2A and C), demonstrating attenuation of CPZ-induced demyelination.

TEM analysis revealed that CPZ elevated the g-ratio (axon diameter/total fiber diameter) compared to NC ($P < 0.001$), reflecting thinner myelin sheaths. Both ZGW-L and ZGW-H treatments reduced the g-ratio versus CPZ ($P < 0.01$; Figure 2B and D), consistent with enhanced myelin sheath thickening. Furthermore, WB quantification of oligodendrocyte differentiation markers, CNPase, MOG, and Olig2, showed significant downregulation in CPZ mice relative to NC ($P < 0.05$). ZGW-H treatment significantly upregulated all three proteins compared to CPZ ($P < 0.05$; Figure 2E–H).

Together, these data indicate that ZGW, particularly at the high dose, mitigates CPZ-induced demyelination and promotes structural and molecular hallmarks of remyelination by driving OPCs differentiation.

Mechanistic Investigation of ZGW Intervention in MS

To ensure quality control and identify bioactive components, LC-MS was employed to systematically profile the ZGW extracts. Analysis was carried out in both positive and negative ion modes. The total ion chromatogram (TIC) is shown in Figure 3. By matching accurate mass (m/z), retention time (RT), fragmentation patterns, and databank data (eg, TCMSP, BATMAN), we preliminarily identified 91 distinct compounds in the ZGW extract (Supplementary Table 1).

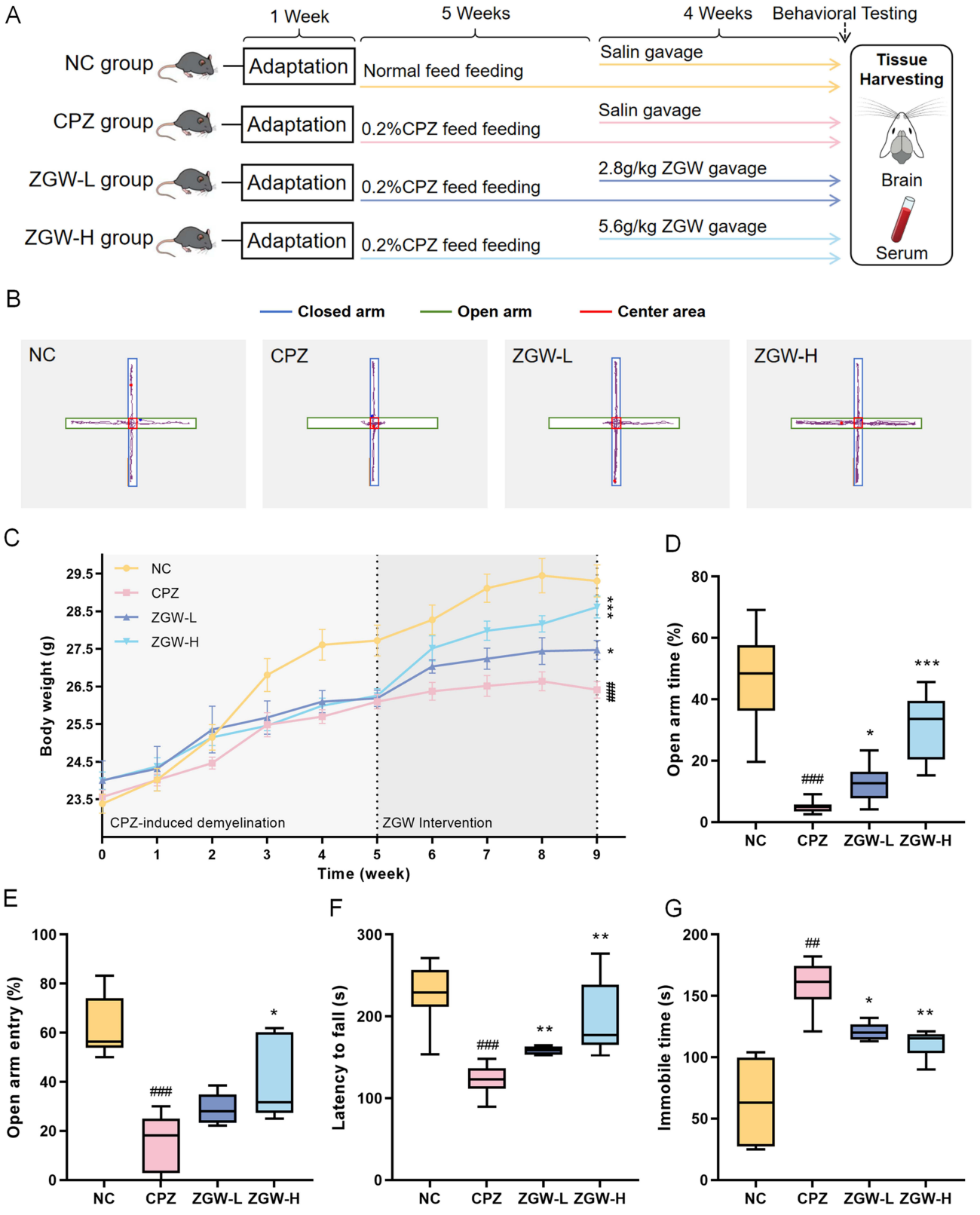

Figure 1 ZGW improves behavioral performance in CPZ-induced demyelinated mice. (**A**) Experimental timeline of the study. (**B**) Body weight change curves. Data are presented as mean ± SEM (**C**) Latency to fall from the rotarod apparatus. (**D**) Representative trajectory plots in the EPM. (**E**) Percentage of total time spent in the open arms of the EPM. (**F**) Percentage of open-arm entries in the EPM (**G**) Immobility time in the TST. *$P < 0.05$, **$P < 0.01$, ***$P < 0.001$ versus CPZ, $^{\#\#}P < 0.01$, $^{\#\#\#}P < 0.001$ versus NC. Data are presented as mean ± SD, except for special notations. (n = 8–10 per group).

https://doi.org/10.2147/JIR.S572873

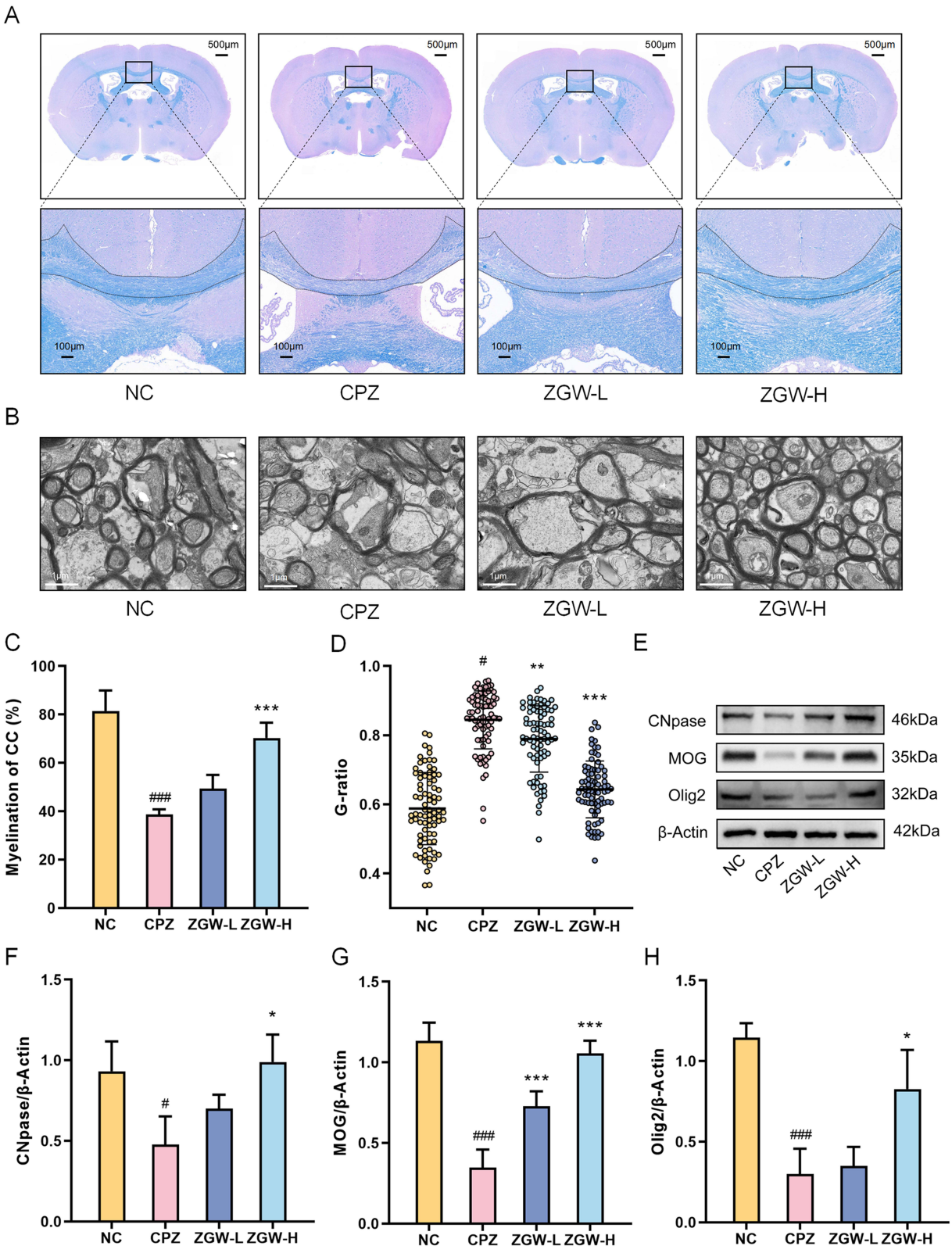

Figure 2 ZGW promotes remyelination in CPZ-induced demyelinated mice. (**A**) Representative LFB staining of the corpus callosum. (**B**) TEM image of the corpus callosum ultrathin sections. (**C**) Quantification of the LFB-positive area in the corpus callosum. (**D**) Myelin g-ratio (axon diameter/total fiber diameter) measured from TEM images. (**E**) Representative Western blots for MOG, Olig2, CNPase, and β-actin (loading control). (**F–H**) Quantification of MOG, Olig2, and CNPase normalized to β-actin. **P* < 0.05, ***P* < 0.01, ****P* < 0.001 versus CPZ, $^{\#}P$ < 0.05, $^{\#\#\#}P$ < 0.001 versus NC. Data are presented as mean ± SD. (n =3 per group).

https://doi.org/10.2147/JIR.S572873

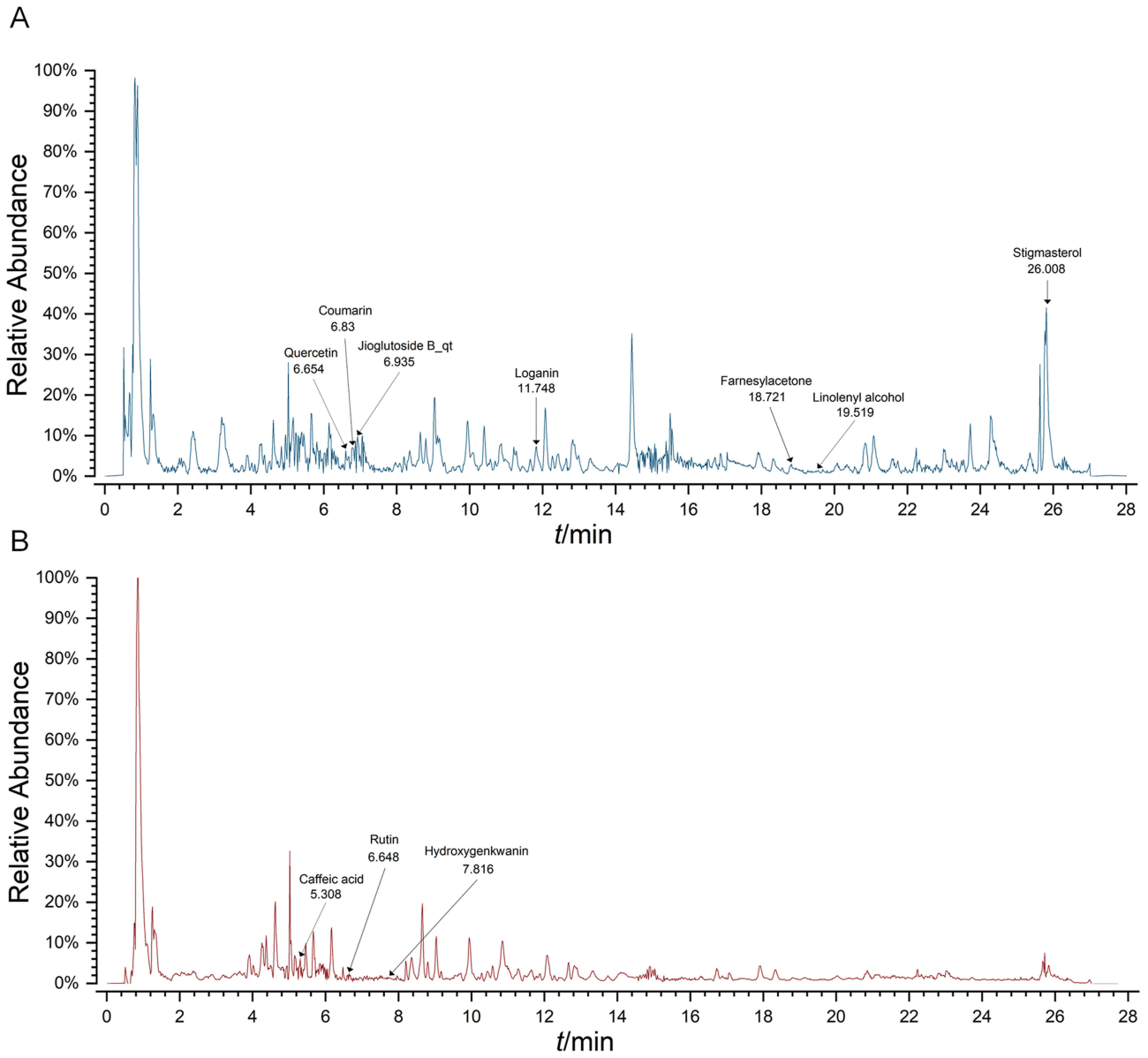

Figure 3 TIC of ZGW extract obtained by LC/MS in the positive (**A**) and negative (**B**) modes.

To uncover the molecular mechanisms underlying ZGW's therapeutic effects, we integrated compound–target data from the TCMSP, BATMAN-TCM, and SwissTargetPrediction databases, yielding 778 putative ZGW targets. Concurrently, 1108 MS-related genes were retrieved from GeneCards, DrugBank, OMIM, TTD, PharmGKB, and GAD databases. A Venn diagram (Figure 4A) identified 228 overlapping targets. Functional enrichment analysis using the DAVID database delineated the biological characteristics of ZGW intervention in MS. GO enrichment analysis (Figure 4B) demonstrated that these targets are primarily involved in, Biological Processes (BP), amino acid metabolism and cellular response to nitrogen compounds. Cellular Components (CC), mitochondrial matrix and dendritic structures. Molecular Functions (MF), oxidoreductase activity and carboxylic acid binding (eg, carboxylate binding). KEGG pathway analysis (Figure 4B) revealed significant enrichment in signaling cascades pertinent to MS pathophysiology, notably the PI3K–Akt and MAPK pathways.

To pinpoint the key molecular drivers, we constructed a high-confidence PPI network (score ≥0.7) of the overlapping targets using STRING 12.0. The resulting network comprised 228 nodes and 5398 edges (Figure 4C). Topological analysis in Cytoscape ranked nodes by Degree, Betweenness and Closeness centrality. The intersection of the top 20 in

https://doi.org/10.2147/JIR.S572873

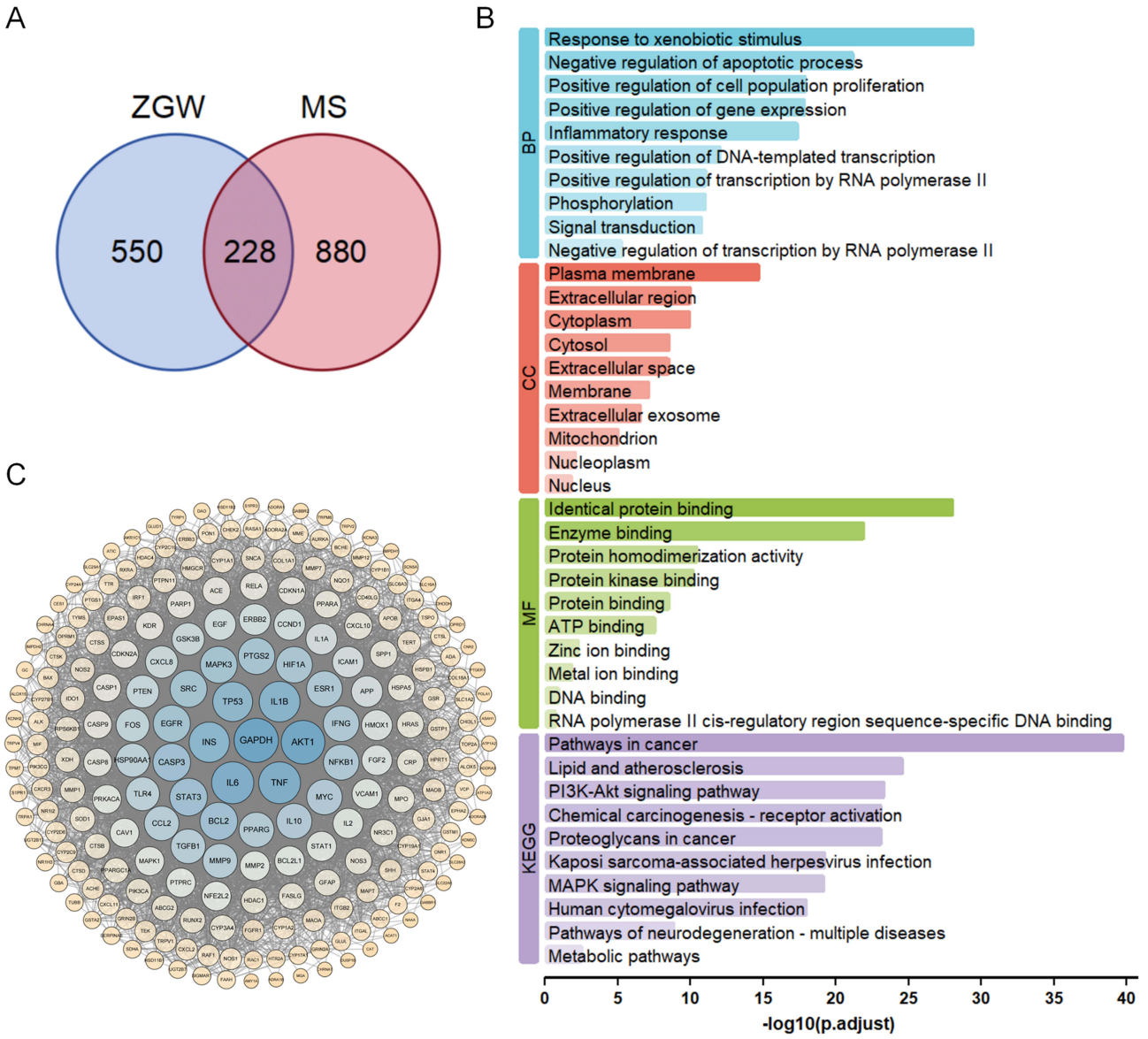

Figure 4 Putative targets and biological characteristics of ZGW intervention in MS. (**A**) Venn diagram showing the intersection of ZGW-related targets (778) and MS-related genes (1108), with 228 common targets. (**B**) GO and KEGG enrichment analysis of the 228 overlapping targets, displayed as the top 10 terms in BP, CC and MF. (**C**) PPI network of the intersecting targets.

each metric yielded 15 hub genes, *GAPDH, AKT1, IL6, TNF, IL1B, INS, TP53, STAT3, BCL2, EGFR, MAPK3, SRC, PTGS2, HIF1A* and *ESR1* (Figures 5A). KEGG enrichment analysis confirmed that these targets predominantly converge on the PI3K-Akt and MAPK pathways (Figure 5B), underscoring these cascades as critical mediators.

To link these core targets back to specific herbal ingredients, a herb-component-target network (327 nodes, 8 herbs, 91 components, 228 targets; 920 edges) was established. Topological screening highlighted the top 10 bioactive components, Quercetin, Caffeic acid, Rutin, Coumarin, Stigmasterol, Farnesylacetone, Loganin, Jioglutoside B_qt, Hydroxygenkwanin, Linolenyl alcohol (Figure 5C and D). These ingredients likely drive ZGW's modulation of the hub proteins and downstream signaling.

Validation via molecular docking showed that all ten high-degree compounds exhibited favorable binding energies (< –7.0 kcal/mol) against the 15 hub proteins (Figure 6A). Notably, Rutin, Stigmasterol and Loganin displayed the strongest predicted affinities toward MAPK pathway mediators, including TNF and MAPK3 (binding modes illustrated in

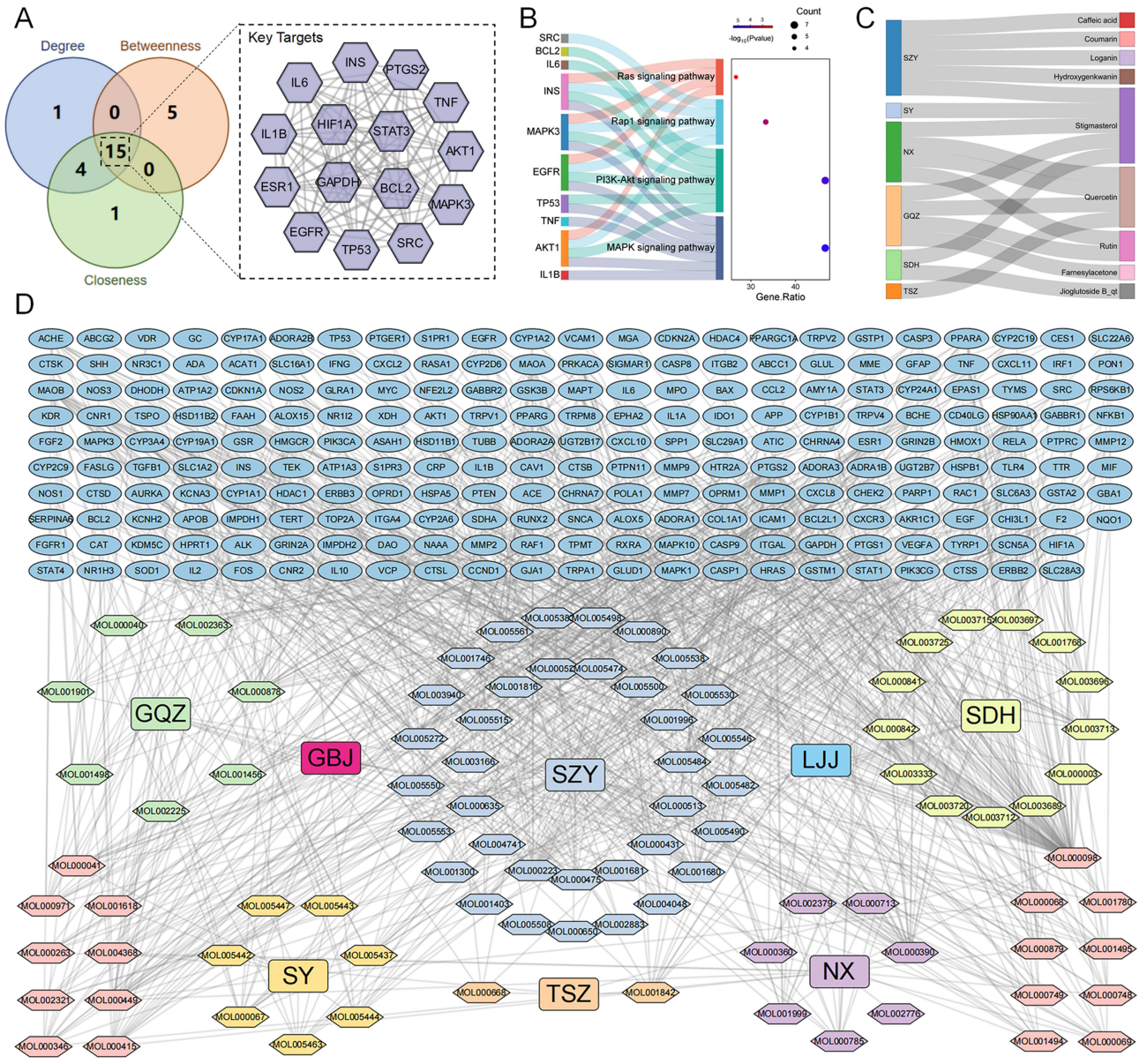

Figure 5 Screening of key components and core targets for ZGW treatment in MS. (**A**) Core target screening based on Degree, Betweenness, and Closeness. (**B**) Enrichment analysis results for core targets. (**C**) Key ingredients - Herbs Sankey diagram. (**D**) Comprehensive herb–component–target network (327 nodes, 920 edges), rectangles represent herbs, hexagons represent active ingredients, and ovals represent targets.

Figure 6B–E). These results corroborate the network pharmacology predictions, supporting these compounds as key modulators of neuroinflammatory signaling.

ZGW Suppresses MAPK Signaling Pathway Activation in CPZ-Induced Demyelinated Mice

To validate the network pharmacology prediction in vivo, we assessed the phosphorylation levels of p38, ERK, and JNK using WB. The CPZ group showed significantly elevated ratios of phospho-p38/total p38, phospho-ERK/total ERK, and phospho-JNK/total JNK compared to the NC group ($P < 0.05$), indicating aberrant activation of the MAPK pathway. In contrast, the ZGW-H group exhibited markedly reduced the phosphorylation ratios of all three MAPK sub-pathways compared to the CPZ group ($P < 0.05$), confirming that ZGW attenuates MAPK pathway overactivation in demyelinated mice. (Figure 7A–D).

https://doi.org/10.2147/JIR.S572873

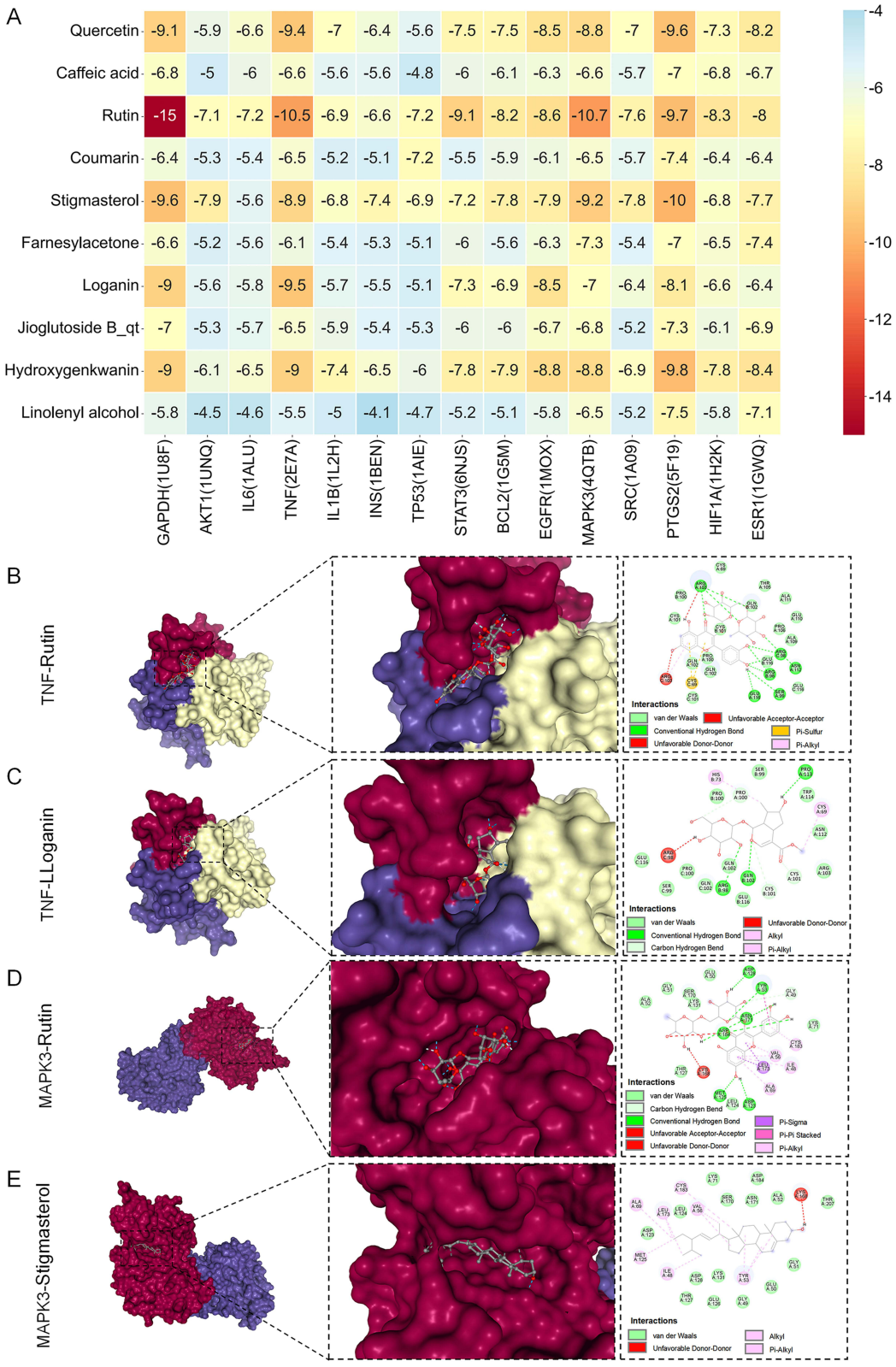

Figure 6 Molecular docking of ZGW bioactives with core MS targets. (**A**) Heatmap of binding energies (kcal/mol) for the top 10 ZGW compounds docked against 15 hub proteins. (**B**–**E**) Representative binding complexes of the compounds with key targets in the MAPK signaling pathway.

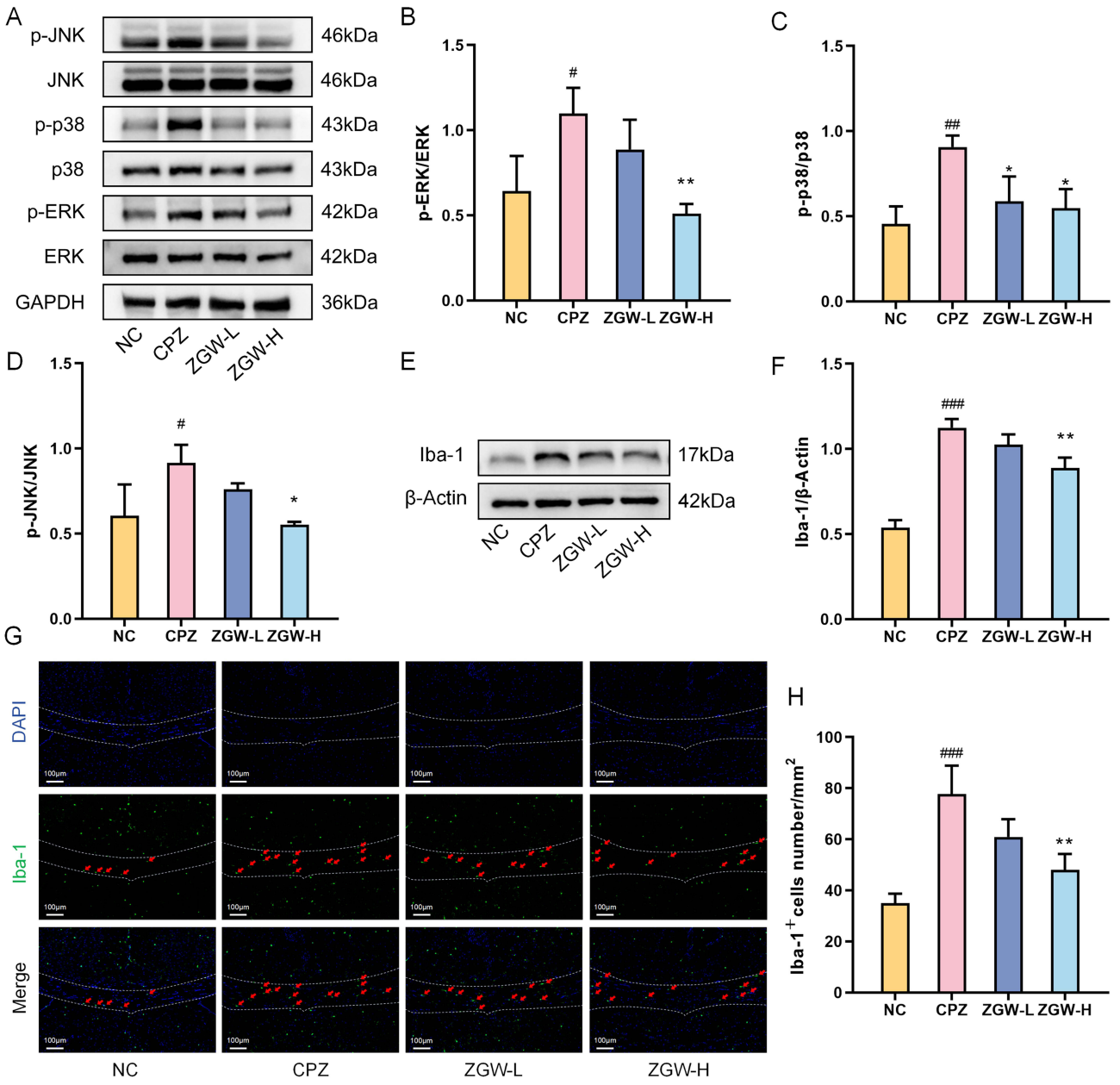

Figure 7 ZGW attenuates MAPK signaling pathway and microglial activation in CPZ-induced demyelinated mice. (**A**) Representative Western blots for phospho-p38, total p38, phospho-ERK1/2, total ERK1/2, phospho-JNK, total JNK, and GAPDH. (**B**–**D**) Quantification of phospho-ERK/ERK (B), phospho-p38/p38 (C), and phospho-JNK/JNK (**D**) ratios. (**E**) Western blots for Iba-1 and β-actin. (**F**) Quantification of Iba-1 normalized to β-actin. (**G**) Representative immunofluorescence for Iba-1$^+$ cells. (**H**) Quantification of Iba-1$^+$ cell density. $^*P < 0.05$, $^{**}P < 0.01$, versus CPZ, $^{\#}P < 0.05$, $^{\#\#}P < 0.01$, $^{\#\#\#}P < 0.001$ versus NC. Data are presented as mean ± SD. (n =3 per group).

ZGW Suppresses Microglial Activation and M1 Polarization in CPZ-Induced Demyelinated Mice

Given the pivotal role of MAPK signaling in microglial activation and polarization, we assessed microglial status and M1/M2 polarization markers. WB analysis (Figure 7E and F) revealed significantly elevated Iba-1 protein levels in the CPZ group compared to NC ($P < 0.001$), which were markedly reduced by ZGW-H treatment ($P < 0.01$). Consistently, immunofluorescence staining (Figure 7G and H) revealed a robust increase in Iba-1$^+$ cell density in CPZ mice versus NC ($P < 0.01$), which was markedly attenuated by ZGW-H ($P < 0.01$).

To dissect whether ZGW differentially modulates microglial M1 versus M2 polarization, we performed concurrent WB and ELISA analyses. WB analysis (Figure 8A–F) revealed that, compared with NC, CPZ markedly upregulated both M1

https://doi.org/10.2147/JIR.S572873

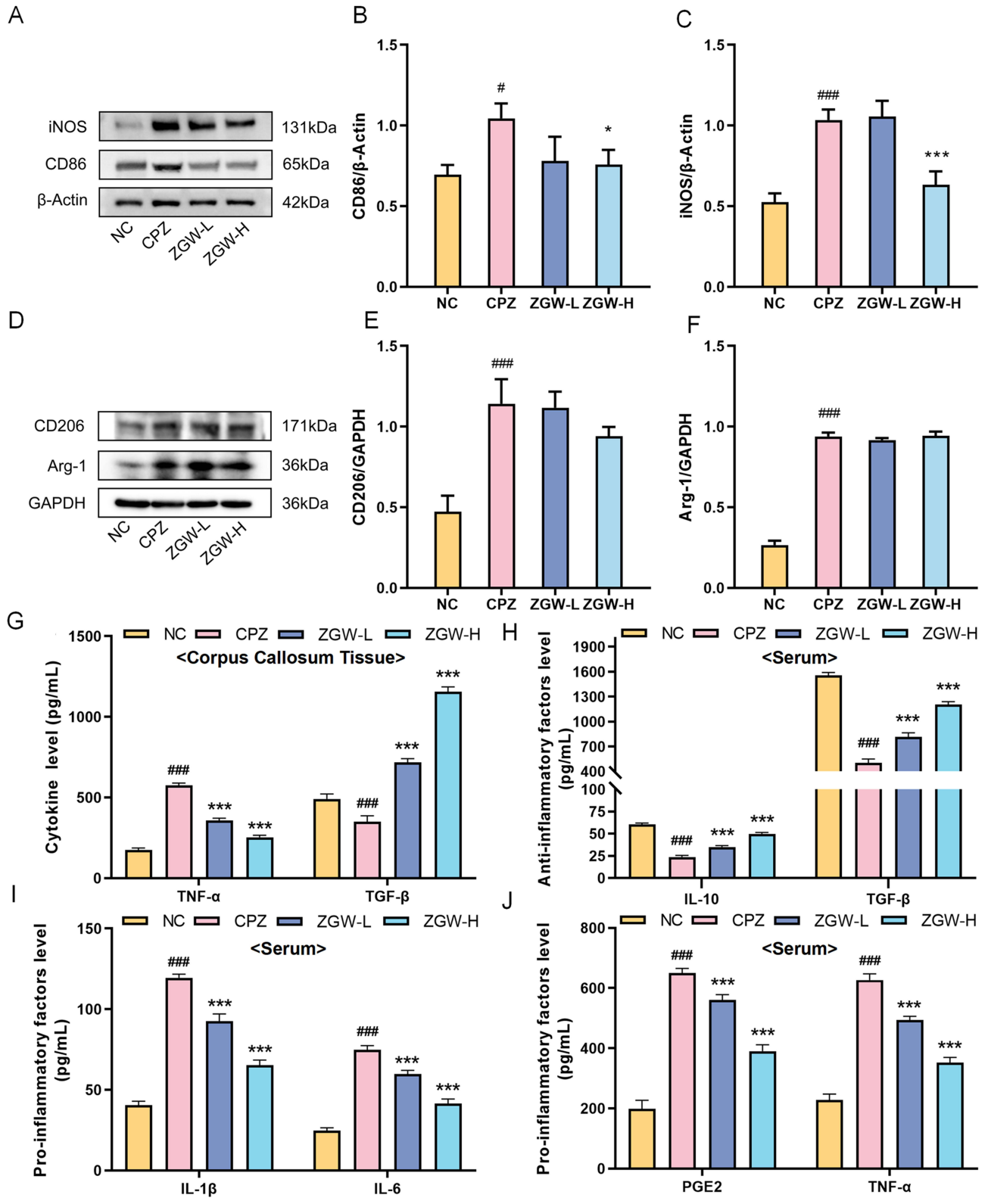

Figure 8 ZGW selectively inhibits microglial M1 polarization in CPZ-induced demyelinated mice. (**A**) Representative Western blots for M1 markers (iNOS and CD86). (**B** and **C**) Quantification of M1 markers normalized to β-actin. (**D**) Representative Western blots for M2 markers (Arg-1 and CD206). (**E** and **F**) Quantification of M2 markers normalized to GAPDH. (**G**) ELISA quantification of TNF-α and TGF-β in corpus callosum lysates. (**H**) Serum concentrations of the anti-inflammatory factors IL-10 and TGF-β. (**I** and **J**) Serum concentrations of pro-inflammatory factors IL-1β, IL-6, TNF-α, and PGE2. $^{*}P < 0.05$, $^{***}P < 0.001$ versus CPZ, $^{\#}P < 0.05$, $^{\#\#\#}P < 0.001$ versus NC. Data are presented as mean ± SD. (n =3 per group for WB and n = 6 per group for ELISA).

https://doi.org/10.2147/JIR.S572873

markers (iNOS, CD86) and M2 markers (CD206, Arg-1) ($P < 0.05$ or $P < 0.001$). Notably, ZGW-H selectively downregulated iNOS and CD86 levels versus CPZ ($P < 0.05$ or $P < 0.001$) without significantly altering CD206 or Arg-1.

ELISA analysis further clarified the functional phenotype. The CPZ induced a pro-inflammatory cytokine profile-elevated TNF-α and reduced TGF-β ($P < 0.001$) relative to NC-indicating an M1-dominant functional state. ZGW treatment significantly suppressed TNF-α secretion and restored TGF-β levels ($P < 0.001$). Furthermore, in serum samples (Figure 8H–J), compared with the NC group, the CPZ group showed significantly elevated pro-inflammatory cytokine (TNF-α, IL-1β, IL-6, PGE2) and reduced anti-inflammatory cytokine levels (TGF-β, IL-10) ($P < 0.001$). In contrast, the ZGW-L and ZGW-H treatments significantly reversed this systemic imbalance ($P < 0.001$), with the ZGW-H group exhibiting the most pronounced effects.

Collectively, these results suggest that ZGW exerts therapeutic effects by specifically inhibiting M1 pro-polarization phenotype and restoring the balance of anti-inflammatory cytokines, rather than by further upregulating M2 protein markers, thus reestablishing immune homeostasis in the demyelinated CNS.

Discussion

In this study, we provided evidence that ZGW, a classical TCM formula, ameliorates demyelination and promotes remyelination in a CPZ-induced mouse model of MS. This effect is achieved by selectively inhibiting microglial M1 polarization via suppression of the MAPK signaling pathway (Figure 9).

This study employs the CPZ-induced murine demyelination model to simulate the demyelination pathology of MS and investigates the mechanism by which ZGW promotes remyelination. CPZ, a copper ion chelator, induces oligodendrocyte apoptosis by disrupting mitochondrial energy metabolism, leading to specific demyelination in the CNS, providing an ideal platform for targeted research on remyelination mechanisms.[13] In the CPZ model, demyelination

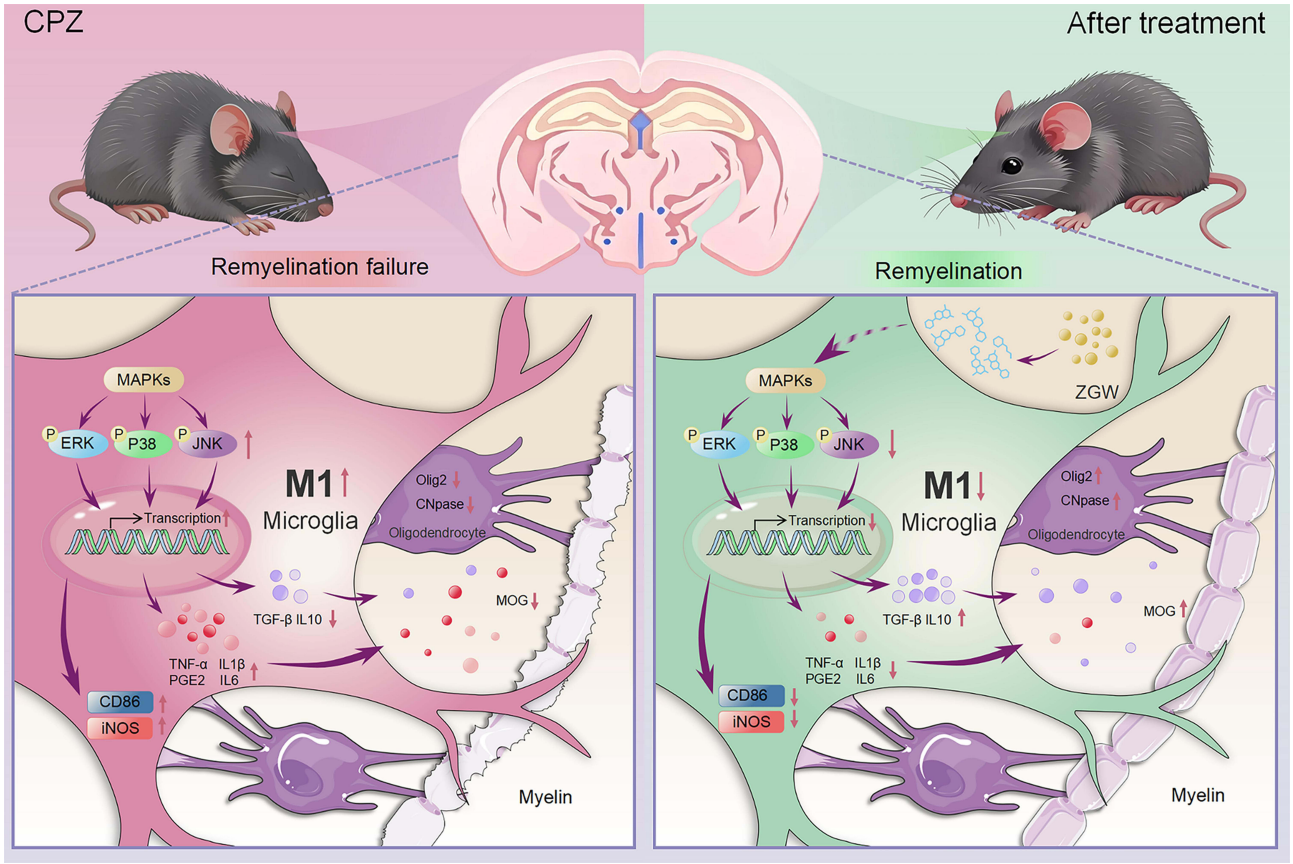

Figure 9 Mechanism of ZGW intervention in MS, ZGW ameliorates MS by suppressing microglial activation and M1 polarization via modulation of the MAPK signaling pathway, thereby promoting remyelination.

https://doi.org/10.2147/JIR.S572873

and neuroinflammation lead to dysfunction in the limbic system (such as the hippocampus and prefrontal cortex), impaired signaling in the cortico-striatal pathway, imbalances in neurotransmitters (such as dopamine and cortisol), and axonal damage, which in turn result in anxiety-like behaviors, depressive phenotypes, and motor dysfunction in mice.[14–20] In our study, CPZ administration induced pronounced weight loss, motor deficits, anxiety- and depressive-like behaviors, all of which were significantly reversed by high-dose ZGW treatment. Active components such as quercetin and stigmasterol in ZGW have now been confirmed to possess anti-anxiety, anti-depressant, and motor function improvement effects.[21–24]

Demyelination is the primary pathological hallmark of MS.[25] Remyelination is a critical reparative process that ameliorates the clinical symptoms of MS.[26,27] Consequently, enhancing remyelination has emerged as a pivotal therapeutic strategy for the management of MS. Histologically, LFB staining and TEM revealed extensive corpus callosum demyelination in CPZ mice, whereas ZGW-treated animals exhibited marked restoration of myelin integrity. The crux of remyelination lies in the differentiation and maturation of OPCs. Under physiological conditions, following demyelination, OPCs migrate to lesion sites, proliferate, and differentiate into mature oligodendrocytes to repair myelin.[28] However, studies of brain tissue from patients with MS have revealed that although OPCs can complete chemotaxis and proliferation, they fail to undergo terminal differentiation and maturation.[29,30] Therefore, OPCs differentiation and maturation are critical for successful remyelination. In this context, we detected key markers of OPCs differentiation and maturation-Olig2, CNPase, and MOG-and demonstrated that ZGW significantly upregulated the expression of these proteins in the corpus callosum. This confirms the role of ZGW in promoting OPCs differentiation and maturation in the CNS.[26] Collectively, these findings demonstrate that ZGW ameliorates neurological dysfunction in CPZ mice by promoting remyelination.

Disease progression in MS is closely associated with the presence of chronic active lesions.[31] Clinically, magnetic resonance imaging (MRI) frequently detects activated microglia/macrophages forming a "paramagnetic rim" at the edge of these expanding lesions.[32,33] In both MS patients and animal models, this aberrant and sustained microglial activation intensifies with disease duration, highlighting microglia as a crucial therapeutic target for halting progression and fostering repair.[34–37] Previous studies support this therapeutic strategy; for instance, oxymatrine has been shown to upregulate the STING/TBK1/IRF3 signaling pathway, reducing microglial infiltration and polarization while promoting IFN-β production to alleviate demyelination in EAE mice.[38] Similarly, Docosahexaenoic acid facilitates the conversion of microglia into a reparative phenotype by promoting LXR-mediated cholesterol recycling, thereby enhancing myelin debris clearance and maintaining white matter integrity in CPZ mice.[39] Thus, regulating microglial polarization represents a promising avenue for remyelination therapy. Consistent with this strategy, our results indicate that ZGW effectively modulated microglial phenotypes. Specifically, ZGW treatment decreased the expression of the activation marker Iba-1 and the M1 polarization markers iNOS and CD86. Functionally, this resulted in a reduction in the pro-inflammatory cytokine TNF-α and an elevation in the anti-inflammatory cytokine TGF-β. Interestingly, classical M2 markers (Arg-1 and CD206) remained unchanged. This suggests that ZGW does not indiscriminately drive a full M2 polarization but rather selectively dampens pathogenic M1 responses. This action effectively shifts the overall microenvironment toward a state permissive for repair, without provoking potential adverse effects that could be linked to overactive M2 states.

To elucidate the molecular driver of this immunomodulation, we employed network pharmacology and identified the MAPK signaling pathway as the core therapeutic target of ZGW. The MAPK cascade is a pivotal regulator of stress responses and inflammation, and its aberrant hyperactivation is a hallmark of MS pathology. Elevated phosphorylation levels of p38 MAPK, JNK, and ERK have been consistently observed in the CNS glial cells of MS patients and EAE mice.[40] This hyperactivation directly drives microglial M1 polarization by engaging downstream transcription factors, such as AP-1 (c-Fos/c-Jun) and NF-κB, which perpetuate the transcription of pro-inflammatory genes (eg, TNF, IL1B, NOS2).[41–43] Conversely, inhibiting p38 or ERK signaling has been shown to attenuate EAE severity and protect against demyelination,[44,45] validating the MAPK axis as a druggable target. Parallel evidence from other inflammatory models supports this mechanism; for example, Berberine has been reported to inhibit the phosphorylation of p38 MAPK and ERK1/2 in the MAPK/NF-κB pathway, thereby promoting a phenotypic shift from M1 to M2 and alleviating hypothalamic inflammation.[46] Our findings demonstrate that ZGW exerts its therapeutic effects precisely by intercepting this pathological signaling. Molecular docking studies revealed that high-degree bioactives in ZGW bind with high affinity to MAPK3 and TNF-α interfaces. These in silico predictions suggest that ZGW components may physically disrupt MAPK

cascade activation and TNF-α stability. Consistent with these predictions, Western blot analysis of corpus callosum tissues confirmed that ZGW markedly reduced the phosphorylation of p38, ERK1/2, and JNK kinases, which were otherwise significantly upregulated by CPZ induction.

This specific profile of broad MAPK inhibition offers a plausible explanation for the observed microglial phenotype (reduced M1, unchanged M2). While p38 and JNK primarily drive M1 programming via NF-κB and AP-1, ERK signaling is more complex, participating in both M1 induction and IL-4/STAT6-mediated M2 skewing.[47–49] By concurrently suppressing all three MAPK arms, ZGW appears to deactivate microglia rather than shifting them to a canonical M2 state. This effectively reduces the functional M1/M2 ratio and permits endogenous TGF-β production-potentially from non-canonical subsets such as disease-associated microglia-to support OPC maturation and myelin repair.[50,51]

Despite these promising findings, several limitations should be acknowledged. First, although network pharmacology identified potential bioactives, the specific active ingredients within the complex ZGW formula were not individually isolated or functionally verified in this study. Second, the association between MAPK inhibition and remyelination is currently correlational; future studies utilizing specific MAPK agonists or genetic knockout models are required to establish definitive causality. Finally, while the CPZ model effectively mimics toxic demyelination, it does not fully recapitulate the autoimmune components of human MS. Further in-depth research is warranted to address these aspects.

Conclusion

In conclusion, this study elucidates a novel mechanism by which ZGW orchestrates microglial deactivation and selective suppression of M1 polarization through the inhibition of the MAPK signaling pathway, thereby facilitating OPC differentiation and remyelination in the CPZ-induced demyelination model. These findings not only provide a mechanistic blueprint for the clinical evaluation of ZGW as a multi-target therapeutic for MS, but also highlight the value of integrating traditional medicine knowledge with modern pharmacology approaches for discovering novel remyelination strategies.

Declaration of Generative AI and AI-Assisted Technologies in the Writing Process

During the preparation of this work, the authors used DeepSeek R1, an AI language model developed by DeepSeek, in order to improve the clarity and wording of the written English. After using this tool, the authors reviewed and edited the content as needed and take full responsibility for the content of the publication.

Materials and Ethics Compliance

The ZGW used is a commercially available, nationally licensed pharmaceutical product manufactured under GMP (Product No., Z41020696; Batch No., 20035036) was supplied by Zhongjing Wanxi Pharmaceutical Co., Ltd. (Henan, China). Its eight ingredients—including Gui Ban Jiao and Lu Jiao Jiao —are sourced from legal suppliers; no endangered or wild-caught animals were sacrificed for this study. This study was reviewed and approved by the Experimental Animal Welfare and Ethics Committee of Henan University of Chinese Medicine, China. The Ethics Approval Code assigned to this study was DWLL202103124.

Abbreviations

ZGW, Zuo Gui Wan; MS, Multiple Sclerosis; CPZ, Cuprizone; EAE, Experimental Autoimmune Encephalomyelitis; TCM, Traditional Chinese Medicine; MAPK, Mitogen-Activated Protein Kinase; PPI, Protein-Protein Interaction; KEGG, Kyoto Encyclopedia of Genes and Genomes; GO, Gene Ontology; BP, Biological Process; CC, Cellular Component; MF, Molecular Function; ERK, Extracellular Signal-Regulated Kinase; p38, p38 Mitogen-Activated Protein Kinase; JNK, c-Jun N-terminal Kinase; Iba-1, Ionized Calcium-Binding Adapter Molecule 1; iNOS, Inducible Nitric Oxide Synthase; Arg-1, Arginase-1; CD86, Cluster of Differentiation 86; CD206, Cluster of Differentiation 206; TNF-α, Tumor Necrosis Factor-alpha; TGF-β, Transforming Growth Factor-beta.

Data Sharing Statement

Data will be made available on request from the corresponding author.

Author Contributions

Peiyuan Zhao (First author), Supervision, Funding acquisition, Resources, Writing - Review & Editing. Yihao Li (Co-first author), Conceptualization, Methodology, Investigation, Writing - Original Draft. Wenlu Li, Conceptualization, Methodology, Writing - Review & Editing. Xu Han, Conceptualization, Methodology, Validation. Weng Cheng, Conceptualization, Resources. Mengyang Fan, Investigation, Writing - Original Draft. Liuqing Xu, Investigation, Writing - Original Draft. Jingxian Han, Investigation, Visualization. Xihong Liu (Corresponding author), Writing - Review & Editing, Project administration. All authors took part in drafting, revising or critically reviewing the article; gave final approval of the version to be published; have agreed on the journal to which the article has been submitted; and agree to be accountable for all aspects of the work.

Funding

This work was financially supported by the National Natural Science Foundation of China (82104579), China Postdoctoral Science Foundation, General Program (2023M731024), Training Programme for Young Backbone Teachers in Higher Education Institutions in Henan Province (2023GGJS080), and Henan University of Chinese Medicine Nursery Project (MP2024-38).

Disclosure

The authors report no conflicts of interest in this work.

References

1. Hauser SL, Cree BAC. Treatment of multiple sclerosis, A review. *Am J Med*. 2020;133(12):1380–1390.e2. doi:10.1016/j.amjmed.2020.05.049
2. Thompson AJ, Baranzini SE, Geurts J, Hemmer B, Ciccarelli O. Multiple sclerosis. *Lancet*. 2018;391(10130):1622–1636. doi:10.1016/S0140-6736(18)30481-1
3. Feigin VL, Nichols E, Alam T, GBD 2016 Neurology Collaborators. Global, regional, and national burden of neurological disorders, 1990–2016, a systematic analysis for the global burden of disease study 2016. *Lancet Neurol*. 2019;18(5):459–480. doi:10.1016/S1474-4422(18)30499-X
4. Stavropoulou De Lorenzo S, Bakirtzis C, Konstantinidou N, et al. How early is early multiple sclerosis? *J Clin Med*. 2023;13(1):214. doi:10.3390/jcm13010214
5. Waldman AT, Gorman MP, Rensel MR, Austin TE, hertz DP, Kuntz NL. Management of pediatric central nervous system demyelinating disorders, consensus of united states neurologists. *J Child Neurol*. 2011;26(6):675–682. doi:10.1177/0883073810395141
6. Yamout B, Sahraian M, Bohlega S, et al. Consensus recommendations for the diagnosis and treatment of multiple sclerosis, 2019 revisions to the MENACTRIMS guidelines. *Mult Scler Relat Disord*. 2020;37:101459. doi:10.1016/j.msard.2019.101459
7. Vidal-Jordana A. New advances in disease-modifying therapies for relapsing and progressive forms of multiple sclerosis. *Neurol Clin*. 2018;36(1):173–183. doi:10.1016/j.ncl.2017.08.011
8. Wang L, Fan YP, Gong HY, et al. Effects of Zuogui Pill and Yougui Pill on myelin and axonal regeneration in rats with experimental allergic encephalomyelitis. *Chin J Exp Tradit Med Form*. 2008;14(4):42–45. doi:10.13422/j.cnki.syfjx.2008.04.019
9. Kent SA, Miron VE. Microglia regulation of central nervous system myelin health and regeneration. *Nat Rev Immunol*. 2024;24(1):49–63. doi:10.1038/s41577-023-00907-4
10. Liddelow SA, Guttenplan KA, Clarke LE, et al. Neurotoxic reactive astrocytes are induced by activated microglia. *Nature*. 2017;541(7638):481–487. doi:10.1038/nature21029
11. Wang YZ, Kou S, Gu LY, et al. Effects of Zuogui Pill and Yougui Pill on the expression of brain-derived neurotrophic factor and cyclic adenosine monophosphate/protein kinase A signaling transduction pathways of axonal regeneration in model rats with experimental autoimmune encephalomyelitis. *Chin J Integr Med*. 2014;20(1):24–30. doi:10.1007/s11655-012-1236-2
12. Sen MK, Mahns DA, Coorssen JR, Shortland PJ. Behavioural phenotypes in the cuprizone model of central nervous system demyelination. *Neurosci Biobehav Rev*. 2019;107:23–46. doi:10.1016/j.neubiorev.2019.08.008
13. Zirngibl M, Assinck P, Sizov A, Caprariello AV, Plemel JR. Oligodendrocyte death and myelin loss in the cuprizone model, an updated overview of the intrinsic and extrinsic causes of cuprizone demyelination. *Mol Neurodegener*. 2022;17(1):34. doi:10.1186/s13024-022-00538-8
14. Paton KF, Hong S, Biggerstaff A, Kivell BM. Sex differences in the behavioural aspects of the cuprizone-induced demyelination model in mice. *Brain Sci*. 2022;12(12):1687. doi:10.3390/brainsci12121687
15. Mahajan VS, Demissie E, Mattoo H, et al. Striking immune phenotypes in gene-targeted mice are driven by a copy-number variant originating from a commercially available C57BL/6 strain. *Cell Rep*. 2016;15(9):1901–1909. doi:10.1016/j.celrep.2016.04.080
16. Yu Q, Hui R, Park J, et al. Strain differences in cuprizone induced demyelination. *Cell Biosci*. 2017;7:59. doi:10.1186/s13578-017-0181-3
17. Rocca MA, Barkhof F, De Luca J, et al. The hippocampus in multiple sclerosis. *Lancet Neurol*. 2018;17(10):918–926. doi:10.1016/S1474-4422(18)30309-0

18. Granberg T, Fan Q, Treaba CA, et al. In vivo characterization of cortical and white matter neuroaxonal pathology in early multiple sclerosis. *Brain*. 2017;140(11):2912–2926. doi:10.1093/brain/awx247
19. Jellinger KA. Behavioral disorders in multiple sclerosis, a comprehensive review. *J Neural Transm*. 2025;132(1):1–22. doi:10.1007/s00702-024-02816-9
20. Cieśla E, Jasińska E, Głuszek-Osuch M, Suliga E. Depressive symptoms in multiple sclerosis, links to body composition, physical activity, and functional ability. *Med Sci Monit*. 2024;30(e943977). doi:10.12659/MSM.943977
21. Teng T, Song C. Research progress of quercetin on anti-anxiety and anti-depression. *Front Pharmacol*. 2025;16:1621510. doi:10.3389/fphar.2025.1621510
22. Chiang MC, Tsai TY, Wang CJ. The potential benefits of quercetin for brain health, a review of anti-inflammatory and neuroprotective mechanisms. *Int J Mol Sci*. 2023;24(7):6328. doi:10.3390/ijms24076328
23. Adebiyi OE, Olopade JO, Olayemi FO. Sodium metavanadate induced cognitive decline, behavioral impairments, oxidative stress and down regulation of myelin basic protein in mice hippocampus, Ameliorative roles of β-spinasterol, and stigmasterol. *Brain Behav*. 2018;8(7):e01014. doi:10.1002/brb3.1014
24. Ghosh S, Kumar A, Sachan N, Chandra P. Evaluation of the antidepressant-like effect of total sterols fraction and stigmasterol isolated from leaves of *Aegle marmelos* and possible mechanism(s) of action involved. *Curr Drug Discov Technol*. 2022;19(2):e290721195144. doi:10.2174/1570163818666210729165310
25. Garton T, Gadani SP, Gill AJ, Calabresi PA. Neurodegeneration and demyelination in multiple sclerosis. *Neuron*. 2024;112(19):3231–3251. doi:10.1016/j.neuron.2024.05.025
26. Zveik O, Rechtman A, Ganz T, Vaknin-Dembinsky A. The interplay of inflammation and remyelination, rethinking MS treatment with a focus on oligodendrocyte progenitor cells. *Mol Neurodegener*. 2024;19(1):53. doi:10.1186/s13024-024-00742-8
27. Goldman SA, Franklin RJM, Osorio J. Stem and progenitor cell-based therapy of myelin disorders. *Handb Clin Neurol*. 2024;205:283–295. doi:10.1016/B978-0-323-90120-8.00015-0
28. Franklin RJM, Bodini B, Goldman SA. Remyelination in the central nervous system. *Cold Spring Harb Perspect Biol*. 2024;16(3):a041371. doi:10.1101/cshperspect.a041371
29. Mezydlo A, Treiber N, Ullrich Gavilanes EM, et al. Remyelination by surviving oligodendrocytes is inefficient in the inflamed mammalian cortex. *Neuron*. 2023;111(11):1748–1759.e8. doi:10.1016/j.neuron.2023.03.031
30. Windener F, Grewing L, Thomas C, et al. Physiological aging and inflammation-induced cellular senescence may contribute to oligodendroglial dysfunction in MS. *Acta Neuropathol*. 2024;147(1):82. doi:10.1007/s00401-024-02733-x
31. Sucksdorff M, Matilainen M, Tuisku J, et al. Brain TSPO-PET predicts later disease progression independent of relapses in multiple sclerosis. *Brain*. 2020;143(11):3318–3330. doi:10.1093/brain/awaa275
32. Dal-Bianco A, Grabner G, Kronnerwetter C, et al. Slow expansion of multiple sclerosis iron rim lesions, pathology and 7 T magnetic resonance imaging. *Acta Neuropathol*. 2017;133(1):25–42. doi:10.1007/s00401-016-1636-z
33. Absinta M, Sati P, Schindler M, et al. Persistent 7-tesla phase rim predicts poor outcome in new multiple sclerosis patient lesions. *J Clin Invest*. 2016;126(7):2597–2609. doi:10.1172/JCI86198
34. Hyvärinen T, Tilvis J, Giudice L, et al. Microglia from patients with multiple sclerosis display a cell-autonomous immune activation state. *J Neuroinflammation*. 2025;22(1):255. doi:10.1186/s12974-025-03575-4
35. Nissen JC, Thompson KK, West BL, Tsirka SE. Csf1R inhibition attenuates experimental autoimmune encephalomyelitis and promotes recovery. *Exp Neurol*. 2018;307:24–36. doi:10.1016/j.expneurol.2018.05.021
36. Absinta M, Maric D, Gharagozloo M, et al. A lymphocyte-microglia-astrocyte axis in chronic active multiple sclerosis. *Nature*. 2021;597(7878):709–714. doi:10.1038/s41586-021-03892-7
37. Heppner FL, Greter M, Marino D, et al. Experimental autoimmune encephalomyelitis repressed by microglial paralysis. *Nature Med*. 2005;11(2):146–152. doi:10.1038/nm1177
38. Wang SS, Jin X, di MW, et al. Oxymatrine regulates microglia to produce IFN-β by activating the STING/TBK1/IRF3 pathway against experimental autoimmune encephalomyelitis. *Eur J Pharmacol*. 2025;1009:178380. doi:10.1016/j.ejphar.2025.178380
39. Liu L, Yang L, Du X, et al. Dihydroartemisinin enhances remyelination by switching microglia to the reparative phenotype. *J Neuroinflammation*. 2025;22(1):197. doi:10.1186/s12974-025-03510-7
40. Krementsov DN, Thornton TM, Teuscher C, Rincon M. The emerging role of p38 mitogen-activated protein kinase in multiple sclerosis and its models. *Mol Cell Biol*. 2013;33(19):3728–3734. doi:10.1128/MCB.00688-13
41. Plastira I, Bernhart E, Joshi L, et al. MAPK signaling determines lysophosphatidic acid (LPA)-induced inflammation in microglia. *J Neuroinflammation*. 2020;17(1):127. doi:10.1186/s12974-020-01809-1
42. Hou X, Qu X, Chen W, et al. CD36 deletion prevents white matter injury by modulating microglia polarization through the Traf5-MAPK signal pathway. *J Neuroinflammation*. 2024;21(1):148. doi:10.1186/s12974-024-03143-2
43. Xu M, Wang J, Zhang X, et al. Polysaccharide from Schisandra chinensis acts via LRP-1 to reverse microglia activation through suppression of the NF-κB and MAPK signaling. *J Ethnopharmacol*. 2020;256:112798. doi:10.1016/j.jep.2020.112798
44. Brereton CF, Sutton CE, Lalor SJ, Lavelle EC, Mills KHG. Inhibition of ERK MAPK suppresses IL-23- and IL-1-driven IL-17 production and attenuates autoimmune disease. *J Iimmunol*. 2009;183(3):1715–1723. doi:10.4049/jimmunol.0803851
45. Noubade R, Krementsov DN, Rio RD, et al. Activation of p38 MAPK in CD4 T cells controls IL-17 production and autoimmune encephalomyelitis. *Blood*. 2011;118(12):3290–3300. doi:10.1182/blood-2011-02-336552
46. Feng Y, Wei Z, Li R, Shi Q, Cai J. Effects and mechanism of berberine in ameliorating microglia-mediated hypothalamic inflammation by downregulating the MAPK and NF-κB pathway. *J Ethnopharmacol*. 2026;355(Pt B):120695. doi:10.1016/j.jep.2025.120695
47. Peng M, Li N, Wang H, et al. Macrophages, subtypes, distribution, polarization, immunomodulatory functions, and therapeutics. *MedComm*. 2025;6(8):e70304. doi:10.1002/mco2.70304
48. Lin MH, Cheng PC, Hsiao PJ, et al. The GLP-1 receptor agonist exenatide ameliorates neuroinflammation, locomotor activity, and anxiety-like behavior in mice with diet-induced obesity through the modulation of microglial M2 polarization and downregulation of SR-A4. *Int Immunopharmacol*. 2023;115:109653. doi:10.1016/j.intimp.2022.109653

49. Gee MS, Kim SW, Kim N, et al. A novel and selective p38 mitogen-activated protein kinase inhibitor attenuates LPS-induced neuroinflammation in BV2 microglia and a mouse model. *Neurochem Res*. 2018;43(12):2362–2371. doi:10.1007/s11064-018-2661-1
50. Deczkowska A, Keren-Shaul H, Weiner A, Colonna M, Schwartz M, Amit I. Disease-associated microglia, A universal immune sensor of neurodegeneration. *Cell*. 2018;173(5):1073–1081. doi:10.1016/j.cell.2018.05.003
51. Hamaguchi M, Muramatsu R, Fujimura H, Mochizuki H, Kataoka H, Yamashita T. Circulating transforming growth factor-β1 facilitates remyelination in the adult central nervous system. *eLife*. 2019;8. doi:10.7554/eLife.41869